The dynamics of starvation and recovery

Justin D. Yeakel [*] [†] [‡], **Christopher P. Kempes** [†], **and Sidney Redner** [†] [§]

[*]School of Natural Science, University of California Merced, Merced, CA,[†]The Santa Fe Institute, Santa Fe, NM,[§]Department of Physics, Boston University, Boston MA, and [‡]To whom correspondence should be addressed: jdyeakel@gmail.com

Submitted to Proceedings of the National Academy of Sciences of the United States of America

The eco-evolutionary dynamics of species is fundamentally linked to the energetic constraints of its constituent individuals. Of particular importance are the tradeoffs between reproduction and the dynamics of starvation and recovery in resource-limited environments. To elucidate the consequences of this tradeoff, we introduce a minimal nutritional state-structured model that incorporates two classes of consumer: nutritionally replete consumers that reproduce, and undernourished, non-reproducing consumers that are susceptible to mortality. As a function of the transition rates between these replete and undernourished states that are determined by the presence or absence of resources, the consumer populations can either undergo cyclic dynamics or reach a steady state. We obtain strong constraints on starvation and recovery rates by deriving allometric scaling relationships and find that population dynamics subject to these constraints can approach the cyclic regime but are typically driven to a steady state. Moreover, we find that these rates fall within a 'refuge' in parameter space, where the probability of extinction of the consumer population is minimized. Thus we identify a potential mechanism that may both drive and constrain the dynamics of animal populations. Our model provides a natural framework that predicts maximum body size for mammals by determining the relative stability of an otherwise homogeneous population to a mutant population with altered percent body fat. For body masses $\lesssim 10^7$g, individuals with increased energetic reserves can invade resident populations, and vice versa for body mass $\gtrsim 10^7$g, thus providing a principled mechanism for a within-lineage driver of Cope's rule.

foraging | starvation | reproduction

Significance Statement Energetic investment in somatic maintenance and growth vs. reproduction directly impacts the dynamics of populations among species. Here, we construct a Nutritional State-structured Model (NSM) to assess the population-level effects of starvation and recovery of a consumer population in a resource-limited environment, and use allometric scaling relationships for mammals to establish all timescales and rates. Our model reveals that mammalian energetic rates minimize the probability of stochastic extinction, establishes dynamic bounds on mammalian body size while providing independent theoretical support for the energy equivalence hypothesis, and provides a mechanistic driver for the evolutionary trend towards larger body size known as Cope's rule.

Introduction

The behavioral ecology of all organisms is influenced by the energetic state of individuals, which directly influences how they invest reserves in uncertain environments. Such behaviors are generally manifested as tradeoffs between investing in somatic maintenance and growth, or allocating energy towards reproduction [1, 2, 3]. The timing of these behaviors responds to selective pressure, as the choice of the investment impacts future fitness [4, 5, 6]. The influence of resource limitation on an organism's ability to maintain its nutritional stores may lead to repeated delays or shifts in reproduction over the course of an organism's life.

The balance between (a) somatic growth and maintenance, and (b) reproduction depends on resource availability [7]. For example, reindeer invest less in calves born after harsh winters (when the mother's energetic state is depleted) than in calves born after moderate winters [8]. Many bird species invest differently in broods during periods of resource scarcity compared to normal periods [9, 10], sometimes delaying or even foregoing reproduction for a breeding season [1, 11, 12]. Even freshwater and marine zooplankton have been observed to avoid reproduction under nutritional stress [13], and those that do reproduce have lower survival rates [2]. Organisms may also separate maintenance and growth from reproduction over space and time: many salmonids, birds, and some mammals return to migratory breeding grounds to reproduce after one or multiple seasons in resource-rich environments where they accumulate nutritional reserves [14, 15, 16].

Physiology also plays an important role in regulating reproductive expenditures during periods of resource limitation. The data collected thus far has shown that diverse mammals (47 species in 10 families) exhibit delayed implantation, whereby females postpone fetal development (blastocyst implantation) until nutritional reserves can be accumulated [17, 18]. Many other many species (including humans) suffer irregular menstrual cycling and higher abortion rates during periods of nutritional stress [19, 20]. In the extreme case of unicellular organisms, nutrition is unavoidably linked to reproduction because the nutritional state of the cell regulates all aspects of the cell cycle [21]. The existence of so many independently evolved mechanisms across such a diverse suite of organisms highlights the importance and universality of the fundamental tradeoff between somatic and reproductive investment. However the general dynamic implications of these constraints are unknown.

Though straightforward conceptually, incorporating the energetic dynamics of individuals [22] into a population-level framework [22, 23] presents numerous mathematical obstacles [24]. An alternative approach involves modeling the macroscale relations that guide somatic versus reproductive investment in a consumer-resource system. For example, macroscale Lotka-Volterra models assume that the growth rate of the consumer population depends on resource density, thus *implicitly* incorporating the requirement of resource availability for reproduction [25].

In this work, we adopt an alternative approach in which we *explicitly* account for resource limitation and the subsequent effects of starvation. Namely, only individuals with sufficient energetic reserves can reproduce. Such a constraint leads to reproductive time lags due to some members of the population going hungry and then recovering. Additionally, we incorporate the idea that reproduction is strongly constrained allometrically [3], and is not generally linearly related to resource density. As we shall show, these constraints influence the ensuing popula-

Reserved for Publication Footnotes

tion dynamics in dramatic ways.

Nutritional state-structured model (NSM)

We begin by defining a minimal Nutritional State-structured population Model (NSM), where the consumer population is partitioned into two states: (a) an energetically replete (full) state F, where the consumer reproduces at a constant rate λ and does not die from starvation, and (b) an energetically deficient (hungry) state H, where the consumer does not reproduce but dies by starvation at rate μ. The underlying resource R evolves by logistic growth with an intrinsic growth rate α and a carrying capacity equal to one. Consumers transition from the full state F to the hungry state H at a rate σ—the starvation rate—and also in proportion to the absence of resources $(1-R)$. Conversely, consumers recover from state H to state F at rate ρ and in proportion to R. Resources are also eaten by the consumers—at rate ρ by hungry consumers and at rate $\beta < \rho$ by full consumers. This inequality accounts for hungry consumers requiring more resources to replace lost body tissue. The NSM represents a fundamental extension of the idealized starving random walk model of foraging, which focuses on resource depletion, to include reproduction and resource replenishment [26, 27, 28].

In the mean-field approximation, in which the consumers and resources are perfectly mixed, their densities evolve according to the rate equations

$$\begin{aligned} \dot{F} &= \lambda F + \rho R H - \sigma\,(1-R)\,F, \\ \dot{H} &= \sigma\,(1-R)\,F - \rho R H - \mu H, \\ \dot{R} &= \alpha R\,(1-R) - (\rho R + P)\,H - \beta F \end{aligned} \qquad [1]$$

This system of nondimensional equations follows from a set of first-principle relationships for resource consumption and growth (please see the supplement for a full derivation and the dimensional form). Notice that the total consumer density $F+H$ evolves according to $\dot{F}+\dot{H} = \lambda F - \mu H$. This resembles the equation of motion for the predator density in the classic Lotka-Volterra model [29], except that the resource density does not appear in the growth term. As discussed above, the attributes of reproduction and mortality have been explicitly apportioned to the full and hungry consumers, respectively, so that the growth in the total density is decoupled from the resource density.

Equation [1] has three fixed points: two trivial fixed points at $(F^*, H^*, R^*) = (0,0,0)$ and $(0,0,1)$, and one non-trivial, internal fixed point at

$$\begin{aligned} F^* &= \frac{\alpha\lambda\mu(\mu+\rho)}{(\lambda\rho+\mu\sigma)(\lambda\rho+\mu\beta)}, \\ H^* &= \frac{\alpha\lambda^2(\mu+\rho)}{(\lambda\rho+\mu\sigma)(\lambda\rho+\mu\beta)}, \\ R^* &= \frac{\mu(\sigma-\lambda)}{\lambda\rho+\mu\sigma}. \end{aligned} \qquad [2]$$

The stability of this fixed point is determined by the Jacobian matrix $\mathbf{J}$, where each matrix element $J_{ij} = \partial\dot{X}_i/\partial X_j$ when evaluated at the internal fixed point, and $\mathbf{X}$ is the vector (F,H,R). The parameters in Eq. [1] are such that the real part of the largest eigenvalue of $\mathbf{J}$ is negative, so that the system is stable with respect to small perturbations from the fixed point. Because this fixed point is unique, it is the global attractor for all population trajectories for any initial condition where the resource and consumer densities are both nonzero.

From Eq. [2], an obvious constraint on the NSM is that the reproduction rate λ must be less than the starvation rate σ, so that R^* is positive. In fact, when the resource density $R = 0$, the rate equation for F gives exponential growth of F for $\lambda > \sigma$. The condition $\sigma = \lambda$ represents a transcritical (TC) bifurcation [30] that demarcates the physical regime from the unphysical regime where F would grow exponentially with time. The biological implication of the constraint $\lambda < \sigma$ has a simple interpretation—the rate at which a macroscopic organism loses mass due to lack of resources is generally much faster than the rate of reproduction. As we will discuss below, this inequality is a natural consequence of allometric constraints [3] for organisms within empirically observed body size ranges.

In the physical regime of $\lambda < \sigma$, the fixed point [2] may either be a stable node or a limit cycle (Fig. 1). In continuous-time systems, a limit cycle arises when a pair of complex conjugate eigenvalues crosses the imaginary axis to attain positive real parts [31]. This Hopf bifurcation is defined by $\mathrm{Det}(\mathbf{S}) = 0$, with $\mathbf{S}$ the Sylvester matrix, which is composed of the coefficients of the characteristic polynomial of the Jacobian matrix [32]. As the system parameters are tuned to be within the stable regime but close to the Hopf bifurcation, the amplitude of the transient but decaying cycles become large. Given that ecological systems are constantly being perturbed [33], the onset of transient cycles, even though they decay with time in the mean-field description, can increase the extinction risk [34, 35, 36]. Thus the distance of a system from the Hopf bifurcation provides a measure of its persistence.

When the starvation rate $\sigma \gg \lambda$, a substantial fraction of the consumers are driven to the hungry non-reproducing state. Because reproduction is inhibited, there is a low steady-state consumer density and a high steady-state resource density. However, if $\sigma/\lambda \to 1$ from above, the population is overloaded with energetically-replete (reproducing) individuals, thereby promoting oscillations between the consumer and resource densities (Fig. 1).

Whereas the relation between consumer growth rate λ and the starvation rate σ defines an absolute bound of biological feasibility—the TC bifurcation—σ also determines the sensitivity of the consumer population to changes in resource density. When $\sigma \gg \lambda$, the steady-state population density is small, thereby increasing the risk of stochastic extinction. On the other hand, as σ decreases, the system will ultimately be poised either near the TC or the Hopf bifurcation (Fig. 1). If the recovery rate ρ is sufficiently small, the TC bifurcation is reached and the resource eventually is eliminated. If ρ exceeds a threshold value, cyclic dynamics will develop as the Hopf bifurcation is approached.

Role of allometry

While there are no a priori constraints on the parameters in the NSM, most organisms correspond to restricted portions of the parameter space. Here we use allometric scaling relations to constrain the covariation of rates in a principled and biologically meaningful manner. Allometric scaling relations highlight common constraints and average trends across large ranges in body size and species diversity. Many of these relations can be derived from a small set of assumptions and below we describe a framework to determine the covariation of timescales and rates across the range of mammals for each of the key parameters of our model (cf. [37]). We are thereby able to define the regime of dynamics occupied by the entire class of mammals along with the key differences between the largest and smallest mammals.

Nearly all of the rates described in the NSM are determined by consumer metabolism, which can be used to describe a variety of organismal features [38]. The scaling relation between an organism's metabolic rate B and its body mass M at reproductive maturity is known to scale as $B = B_0 M^{\eta}$ [39], where the scaling exponent η is typically close to 2/3 or 3/4 for metazoans (e.g., [38]), and has taxonomic shifts for unicellular species be-

tween $\eta \approx 1$ in eukaryotes and $\eta \approx 1.76$ in bacteria [40, 3]. An organism's metabolic rate B is proportional to the cost of tissue maintenance in the absence of growth (i.e., when the body mass is M). By definition $B = \beta/\xi$, where β is the rate at which resources are consumed for full consumers (see Eq. [**1**]) and where ξ is related to the conversion efficiency of resource to consumer tissue (Supporting Information).

Several efforts have shown how a partitioning of B between growth and maintenance purposes can be used to derive a general equation for both the growth trajectories and growth rates of organisms ranging from bacteria to metazoans [41, 42, 43, 44, 3]. This relation is derived from the simple balance condition [41, 42, 43, 44, 3]

$$B_0 m^\eta = E_m \dot{m} + B_m m\,, \qquad [\mathbf{3}]$$

where E_m is the energy needed to synthesize a unit of mass, B_m is the metabolic rate to support an existing unit of mass, and m is the mass of the organism at any point in its development. This balance has the general solution [45, 3]

$$\left(\frac{m\,(t)}{M}\right)^{1-\eta} = 1 - \left[1 - \left(\frac{m_0}{M}\right)^{1-\eta}\right] e^{-a(1-\eta)t/M^{1-\eta}} \qquad [\mathbf{4}]$$

where, for $\eta < 1$, $M = (B_0/B_m)^{1/(1-\eta)}$ is the asymptotic mass, $a = B_0/E_m$, and m_0 is mass at birth. We now use this solution to define the timescale of reproduction and recovery from starvation (Fig. 2; see [42] for a detailed presentation of these timescales). The time that it takes to reach a particular mass ϵM is given by the timescale

$$\tau\,(\epsilon) = \ln\left[\frac{1 - (m_0/M)^{1-\eta}}{1 - \epsilon^{1-\eta}}\right] \frac{M^{1-\eta}}{a\,(1-\eta)} \qquad [\mathbf{5}]$$

where we will define values of ϵ to describe a set of rates within our model. For the time to reproduce, $t_\lambda = \tau\,(\epsilon_\lambda)$, where ϵ_λ is the fraction of the asymptotic mass where an organism is reproductively mature and should be close to one (typically $\epsilon_\lambda \approx 0.95$ [41]). The growth rate is then given by $\lambda = \ln(\upsilon)\,/t_\lambda$ where υ is the number of offspring produced, and for any constant value of ϵ_λ this will scale like $\lambda \propto M^{\eta-1}$ for $M >> m_0$ [41, 42, 43, 44, 3].

The rate of recovery $\rho = 1/t_\rho$ requires that an organism accrues sufficient tissue to transition from the hungry to the full state. Since only certain tissues can be digested for energy (for example the brain cannot be degraded to fuel metabolism), we define the rates for starvation, death, and recovery by the timescales required to reach, or return from, specific fractions of the replete-state mass (Fig. 3; see Supporting Information, Table I for parameterizations). We define $m_\sigma = \epsilon_\sigma M$, where $\epsilon_\sigma < 1$ is the fraction of replete-state mass where reproduction ceases. This fraction will be modified if tissue composition systematically scales with adult mass. For example, making use of the observation that body fat in mammals scales with overall body size according to $M_{\rm fat} = f_0 M^\gamma$ and assuming that once this mass is fully digested the organism starves, this would imply that $\epsilon_\sigma = 1 - f_0 M^\gamma/M$. It follows that the recovery timescale, t_ρ, is the time to go from $m = \epsilon_\sigma \epsilon_\lambda M$ to $m = \epsilon_\lambda M$ (Fig. 2). Using Eqs. [**4**] and [**5**] this timescale is given by simply considering an adjusted starting mass of $m_0' = \epsilon_\sigma \epsilon_\lambda M$, in which case

$$t_\rho = \ln\left[\frac{1 - (\epsilon_\sigma \epsilon_\lambda)^{1-\eta}}{1 - \epsilon^{1-\eta}}\right] \frac{M^{1-\eta}}{a'\,(1-\eta)} \qquad [\mathbf{6}]$$

where $a' = B_0/E_m'$ accounts for possible deviations in the biosynthetic energetics during recovery (see Supporting Information). It should be noted that more complicated ontogenetic models explicitly handle storage [44], whereas this feature is implicitly covered by the body fat scaling in our framework.

To determine the starvation rate, σ, we are interested in the time required for an organism to go from a mature adult that reproduces at rate λ, to a reduced-mass hungry state where reproduction is impossible. For starving individuals we assume that an organism must meet its maintenance requirements using the digestion of existing mass as the sole energy source. This assumption implies the following simple metabolic balance

$$\dot{m} E_m' = -B_m m \qquad [\mathbf{7}]$$

or

$$\dot{m} = -\frac{a'}{M^{1-\eta}} m \qquad [\mathbf{8}]$$

where E_m' is the amount of energy stored in a unit of existing body mass which differs from E_m, the energy required to synthesis a unit of biomass [44]. Given the replete mass, M, of an organism, the above energy balance prescribes the mass trajectory of a non-consuming organism:

$$m\,(t) = M e^{-a' t/M^{1-\eta}}. \qquad [\mathbf{9}]$$

The time scale for starvation is given by the time it takes $m(t)$ to reach $\epsilon_\sigma M$, which gives

$$t_\sigma = -\frac{M^{1-\eta}}{a'} \ln\,(\epsilon_\sigma)\,. \qquad [\mathbf{10}]$$

The starvation rate is then $\sigma = 1/t_\sigma$, which scales with replete-state mass as $1/M^{1-\eta} \ln\,(1 - f_0 M^\gamma/M)$. An important feature is that σ does not have a simple scaling dependence on λ (Fig. 3), which is important for the dynamics that we later discuss.

The time to death should follow a similar relation, but defined by a lower fraction of replete-state mass, $m_\mu = \epsilon_\mu M$. Suppose, for example, that an organism dies once it has digested all fat and muscle tissues, and that muscle tissue scales with body mass according to $M_{\rm musc} = u_0 M^\zeta$. This gives $\epsilon_\mu = 1 - \left(f_0 M^\gamma + u_0 M^\zeta\right)/M$. Muscle mass has been shown to be roughly proportional to body mass [46] in mammals and thus ϵ_μ is merely ϵ_σ minus a constant. The time to death is the total time to reach $\epsilon_\mu M$ minus the time to starve, or

$$t_\mu = -\frac{M^{1-\eta}}{a'} \ln\,(\epsilon_\mu) - t_\sigma, \qquad [\mathbf{11}]$$

and $\mu = 1/t_\mu$.

Although the rate equations [**1**] are general, here we focus on parameterizations for terrestrial-bound endotherms, specifically mammals, which range from a minimum of $M \approx 1$g (the Etruscan shrew *Suncus etruscus*) to a maximum of $M \approx 10^7$g (the late Eocene to early Miocene Indricotheriinae). Investigating other classes of organisms would simply involve altering the metabolic exponents and scalings associate with ϵ. Moreover, we emphasize that our allometric equations describe mean relationships, and do not account for the (sometimes considerable) variance associated with individual species.

Stabilizing effects of allometric constraints

As the allometric derivations of the NSM rate laws reveal, starvation and recovery rates are not independent parameters, and the biologically relevant portion of the phase space shown in Fig. 1 is constrained via covarying parameters. Given the parameters of terrestrial endotherms, we find that the starvation rate σ and the recovery rate ρ are constrained to lie within a small window of potential values (Fig. 4) for the known range of body sizes M. We thus find that the dynamics for all mammalian body sizes is confined to the steady-state regime of the NSM and that limit-cycle behavior is precluded. Moreover, for larger M, the distance to the Hopf bifurcation increases, while

uncertainty in allometric parameters (20% variation around the mean; Fig. 4) results in little qualitative difference in the distance to the the Hopf bifurcation. These results suggest that small mammals are more prone to population oscillations—both stable limit cycles and transient cycles—than mammals with larger body size. Thus our NSM model predicts that population cycles should be less common for larger species and more common for smaller species, particularly in environments where resources are limiting.

It should be noted that previous studies have used allometric constraints to explain the periodicity of cyclic populations [47, 48, 49], suggesting a period $\propto M^{0.25}$. However this relation seems to hold only for some species [50], and potential drivers range from predator and/or prey lifespans to competitive dynamics [51, 52]. Statistically significant support for the existence of population cycles among mammals is predominantly based on time series for small mammals [53], in agreement with our predictions of more pronounced transient dynamics, given how close these points are to the Hopf bifurcation. On the other hand, the longer gestational times and the increased difficulty in measurements, precludes obtaining similar-quality data for larger organisms.

Extinction risk

Within our model, higher rates of starvation result in a larger flux of the population to the hungry state. In this state reproduction is absent, thus increasing the likelihood of extinction. From the perspective of population survival, it is the rate of starvation relative to the rate of recovery that determines the long-term dynamics of the various species (Fig. 1). We therefore examine the competing effects of cyclic dynamics vs. changes in steady state density on extinction risk as a function of σ and ρ. To this end, we computed the probability of extinction, where we define extinction as a population trajectory falling below one tenth of the allometrically constrained steady state at any time between $t = 10^5$ and $t \leq 10^8$. This procedure is repeated for 1000 replicates of the continuous-time system shown in Eq. 1 for an organism of $M = 100$ grams. In each replicate the initial densities are chosen to be $A(F^*, H^*, R^*)$, with A a random variable that is uniformly distributed in $[0, 2]$. By allowing the rate of starvation to vary, we assessed extinction risk across a range of values for σ and ρ between ca. 10^{-6} to 10^{-1}. As expected, higher rates of extinction correlate with both high values of σ if ρ is small, and high values of ρ if σ is small. For low values of σ and high values of ρ, the increased extinction risk results from transient cycles with larger amplitudes as the system nears the Hopf bifurcation (Fig. 5). For high values of σ and low values of ρ, higher extinction risk arises because of the decrease in the steady state consumer population density (Figs. 1*B*, 5). This interplay creates an 'extinction refuge', such that for a constrained range of σ and ρ, extinction probabilities are minimized.

We find that the allometrically constrained values of σ and ρ fall squarely within the extinction refuge (Fig. 5, white point). These values are close enough to the Hopf bifurcation to avoid low steady state densities, and far enough away to avoid large-amplitude transient cycles. The fact that allometric values of σ and ρ fall within this relatively small window supports the possibility that a selective mechanism has constrained the physiological conditions that drive starvation and recovery rates within populations. Such a mechanism would select for organism physiology that generates appropriate σ and ρ values that serve to minimize extinction risk. This selection could occur via the tuning of body fat percentages, metabolic rates, and biomass maintenance efficiencies. To summarize, our finding that the allometrically-determined parameters fall within this low extinction probability region suggests that the NSM dynamics may both drive—and constrain—natural animal populations.

Dynamic and energetic barriers to body size

Metabolite transport constraints are widely thought to place strict boundaries on biological scaling [54, 55, 38] and thereby lead to specific predictions on the minimum possible body size for organisms [56]. Above this bound, a number of energetic and evolutionary mechanisms have been explored to assess the costs and benefits associated with larger body masses, particularly for mammals. One important such example is the *fasting endurance hypothesis*, which contends that larger body size, with consequent lower metabolic rates and increased ability to maintain more endogenous energetic reserves, may buffer organisms against environmental fluctuations in resource availability [57]. Over evolutionary time, terrestrial mammalian lineages show a significant trend towards larger body size (known as Cope's rule) [58, 59, 60, 61], and it is thought that within-lineage drivers generate selection towards an optimal upper bound of roughly 10^7 grams [58], a value that is likely limited by higher extinction risk for large taxa over longer timescales [59]. These trends are thought to be driven by a combination of climate change and niche availability [61]; however the underpinning energetic costs and benefits of larger body sizes, and how they influence dynamics over ecological timescales, have not been explored. We argue that the NSM provides a suitable framework to explore these issues.

The NSM correctly predicts that species with smaller masses have larger steady-state population densities (Fig. 6*A*). Moreover, we show that the NSM provides independent theoretical support for the energy equivalence hypothesis [62, 63]. The energy equivalence hypothesis argues that the total energy use, B_{tot}, of a population is constant independent of species size (e.g. [62, 63]). This hypothesis is based on observations showing that the abundance, N, of a species is proportional to the inverse of individual metabolism (e.g. $N \propto M^{-3/4}/B_0$) (e.g. [62, 63]). This is usually stated as $B_{tot} = NB = C$ where C is a constant, and has been shown to hold in both mammalian and vascular plant communities [62, 63]. Figure 6*A* shows that both F^* and H^* scale like $M^{-\eta}$ over a wide range of organism sizes and Figure 6*B* shows that F^*B is nearly constant over this same range. This result if remarkable because it illustrates that the steady state values of the NSM combined with the derived timescales naturally give rise to the energy equivalence result. Our model shows that the equivalence breaks down at the maximum observed body sizes for mammals, suggesting that this is a hard limit where deviations outside of this range are energetically suboptimal. A stronger version of this statement is that the total metabolic rate of F and H becomes infinite at a finite mass, occuring at the same scale where the steady state resources vanish (Fig. 6). This asymptotic behavior represents an upper bound on mammalian body size and occurs at $M_{max} = VALUE$. Moreover, $M_{\max}$, which is entirely determined by the population-level consequences of energetic constraints, is remarkably close to the maximum body size observed in the North American mammalian fossil record [58] as well as the mass predicted from an evolutionary model of body size evolution [59].

We contend that the NSM provides a mechanistic understanding of the energetic dynamics that give rise to both observed limitations on mammalian body size as well as the observed trend towards larger body size over evolutionary time. The NSM predicts that the steady state resource density R^* decreases with increasing body size of the consumer population (Fig. 6*C*), and classic resource competition theory predicts that the species surviving on the lowest resource abundance will outcompete others [64, 65, 66]. Thus, the combined NSM steady-

state dynamics and allometric timescales predict that larger mammals have an intrinsic competitive advantage given a common resource, but does not offer a within-lineage mechanism by which larger body sizes are selected for.

To examine whether the NSM could provide such a mechanism, we begin by noting that a theoretical upper bound on mammalian body size is given by $\epsilon_\sigma = 0$, where mammals are entirely composed of metabolic reserves, and this occurs at $M = 8.3 \times 10^8$, or 4.5× the mass of a blue whale. Next we examine to what extent a more realistic upper bound to body mass may serve as an evolutionary attractor, thus providing a suitable within-linneage mechanism for Cope's rule. We directly assess the susceptibility of an otherwise homogeneous population to invasion by a mutated subset of the population (denoted by $'$) where individuals have a modified proportion of body fat $M' = M(1+\chi)$ where $\chi \in [-1, 1]$, thus altering the rates of starvation $\sigma(M')$, recovery $\rho(M')$, and maintenance $\beta(M')$. There is no internal fixed point corresponding to a state where both original residents and invaders coexist (except for the trivial state $\chi = 0$). To assess the susceptibility to invasion as a function of the invader mass, we determine which consumer has a lower steady-state resource density for a given value of χ. We find that for $1 \leq M < VALUEg$, having additional body fat ($\chi > 0$) results in a higher steady-state invader population density ($H'^* + F'^* > H^* + F^*$). Thus the invader has an intrinsic advantage over the resident population. However, for $M > VALUE$, leaner individuals ($\chi < 0$) have advantageous steady state densities.

The observed switch in susceptibility as a function of χ at $M_{\rm opt} = VALUE$ thus serves as an attractor, or an uninvadible evolutionary stable state, such that the NSM predicts organismal mass to increase if $M < M_{\rm opt}$ and decrease if $M > M_{\rm opt}$. This value is close to but smaller than the asymptotic upper bound for terrestrial mammal size predicted by the NSM and is also remarkable close to independent estimates of the largest land mammal [58, 59].

While the state of the environment, as well as the competitive landscape, will determine whether specific body sizes are selected for or against [61], we suggest that the dynamics of starvation and recovery described in the NSM may provide a general driving mechanism for the evolution of larger body size among terrestrial mammals.

The energetics associated with somatic maintenance, growth, and reproduction are important elements that influence the dynamics of all populations [11]. The NSM is a minimal and general model that incorporates the dynamics of starvation and recovery that are expected to occur in resource-limited environments. By incorporating allometric relations between the rates in the NSM, we found: (i) different organismal masses have distinct population dynamic regimes, (ii) allometrically-determined rates of starvation and recovery appear to minimize extinction risk, and (iii) the dynamic consequences of these rates may introduce additional drivers and hard boundaries on the evolution of minimum and maximum body size. We suggest that the NSM offers a means by which the dynamic consequences of energetic constraints can be assessed using macroscale interactions between and among species. Future efforts will involve exploring the consequences of these dynamics in a spatially explicit framework, thus incorporating elements such as movement costs and spatial heterogeneity, which may elucidate additional tradeoffs associated with the dynamics of starvation and recovery.

1. Martin TE (1987) Food as a Limit on Breeding Birds: A Life-History Perspective. *Annu. Rev. Ecol. Syst.* 18:453–487.
2. Kirk KL (1997) Life-History Responses to Variable Environments: Starvation and Reproduction in Planktonic Rotifers. *Ecology* 78:434–441.
3. Kempes CP, Dutkiewicz S, Follows MJ (2012) Growth, metabolic partitioning, and the size of microorganisms. *PNAS* 109:495–500.
4. Mangel M, Clark CW (1988) *Dynamic Modeling in Behavioral Ecology* (Princeton University Press, Princeton).
5. Mangel M (2014) Stochastic dynamic programming illuminates the link between environment, physiology, and evolution. *B. Math. Biol.* 77:857–877.
6. Yeakel JD, Dominy NJ, Koch PL, Mangel M (2014) Functional morphology, stable isotopes, and human evolution: a model of consilience. *Evolution* 68:190–203.
7. Morris DW (1987) Optimal Allocation of Parental Investment. *Oikos* 49:332.
8. Tveraa T, Fauchald P, Henaug C, Yoccoz NG (2003) An examination of a compensatory relationship between food limitation and predation in semi-domestic reindeer. *Oecologia* 137:370–376.
9. Daan S, Dijkstra C, Drent R, Meijer T (1988) *Food supply and the annual timing of avian reproduction.*
10. Jacot A, Valcu M, van Oers K, Kempenaers B (2009) Experimental nest site limitation affects reproductive strategies and parental investment in a hole-nesting passerine. *Animal Behaviour* 77:1075–1083.
11. Stearns SC (1989) Trade-Offs in Life-History Evolution. *Funct. Ecol.* 3:259.
12. Barboza P, Jorde D (2002) Intermittent fasting during winter and spring affects body composition and reproduction of a migratory duck. *J Comp Physiol B* 172:419–434.
13. Threlkeld ST (1976) Starvation and the size structure of zooplankton communities. *Freshwater Biol.* 6:489–496.
14. Weber TP, Ens BJ, Houston AI (1998) Optimal avian migration: A dynamic model of fuel stores and site use. *Evolutionary Ecology* 12:377–401.
15. Mduma SAR, Sinclair ARE, Hilborn R (1999) Food regulates the Serengeti wildebeest: a 40-year record. *J. Anim. Ecol.* 68:1101–1122.
16. Moore JW, Yeakel JD, Peard D, Lough J, Beere M (2014) Life-history diversity and its importance to population stability and persistence of a migratory fish: steelhead in two large North American watersheds. *J. Anim. Ecol.* 83:1035–1046.
17. Mead RA (1989) in *Carnivore Behavior, Ecology, and Evolution* (Springer US, Boston, MA), pp 437–464.
18. Sandell M (1990) The Evolution of Seasonal Delayed Implantation. *The Quarterly Review of Biology* 65:23–42.
19. Bulik CM, et al. (1999) Fertility and Reproduction in Women With Anorexia Nervosa. *J. Clin. Psychiatry* 60:130–135.
20. Trites AW, Donnelly CP (2003) The decline of Steller sea lions Eumetopias jubatus in Alaska: a review of the nutritional stress hypothesis. *Mammal Review* 33:3–28.
21. Glazier DS (2009) Metabolic level and size scaling of rates of respiration and growth in unicellular organisms. *Funct. Ecol.* 23:963–968.
22. Kooijman SALM (2000) *Dynamic Energy and Mass Budgets in Biological Systems* (Cambridge).
23. Sousa T, Domingos T, Poggiale JC, Kooijman SALM (2010) Dynamic energy budget theory restores coherence in biology. *Philos. T. Roy. Soc. B* 365:3413–3428.
24. Diekmann O, Metz JAJ (2010) How to lift a model for individual behaviour to the population level? *Philos. T. Roy. Soc. B* 365:3523–3530.
25. Murdoch WW, Briggs CJ, Nisbet RM (2003) *Consumer-resource Dynamics*, Monographs in population biology (Princeton University Press).
26. Benichou O, Redner S (2014) Depletion-Controlled Starvation of a Diffusing Forager. *arXiv*.
27. Bénichou O, Chupeau M, Redner S (2016) Role of Depletion on the Dynamics of a Diffusing Forager.
28. Chupeau M, Bénichou O, Redner S (2016) Universality classes of foraging with resource renewal. *Phys. Rev. E* 93:032403.
29. Murray JD (2011) *Mathematical Biology: I. An Introduction*, Interdisciplinary Applied Mathematics (Springer New York, Melaka Manipal Medical College (Manipal Campus), International Centre for Health Sciences, Madhav Nagar, Manipal, Udupi District, Karnataka State, India. nayaksathish@yahoo.com) Vol. 110.
30. Strogatz SH (2008) *Nonlinear Dynamics and Chaos*, With Applications to Physics, Biology, Chemistry, and Engineering (Westview Press).
31. Guckenheimer J, Holmes P (1983) *Nonlinear oscillations, dynamical systems, and bifurcations of vector fields* (Springer, New York).
32. Gross T, Feudel U (2004) Analytical search for bifurcation surfaces in parameter space. *Physica D* 195:292–302.
33. Hastings A (2001) Transient dynamics and persistence of ecological systems. *Ecol. Lett.* 4:215–220.
34. Neubert M, Caswell H (1997) Alternatives to resilience for measuring the responses of ecological systems to perturbations. *Ecology* 78:653–665.
35. Caswell H, Neubert MG (2005) Reactivity and transient dynamics of discrete-time ecological systems. *Journal of Difference Equations and Applications* 11:295–310.
36. Neubert M, Caswell H (2009) Detecting reactivity. *Ecology*.
37. Yodzis P, Innes S (1992) Body Size and Consumer-Resource Dynamics. *Am. Nat.* 139:1151–1175.
38. Brown J, Gillooly J, Allen A, Savage V, West G (2004) Toward a metabolic theory of ecology. *Ecology* 85:1771–1789.
39. West GB, Woodruff WH, Brown JH (2002) Allometric scaling of metabolic rate from molecules and mitochondria to cells and mammals. *Proc. Natl. Acad. Sci. USA* 99 Suppl 1:2473–2478.

40. DeLong JP, Okie JG, Moses ME, Sibly RM, Brown JH (2010) Shifts in metabolic scaling, production, and efficiency across major evolutionary transitions of life. *PNAS* 107:12941–12945.
41. West GB, Brown JH, Enquist BJ (2001) A general model for ontogenetic growth. *Nature* 413:628–631.
42. Moses ME, et al. (2008) Revisiting a Model of Ontogenetic Growth: Estimating Model Parameters from Theory and Data. *http://dx.doi.org.proxy.lib.sfu.ca/10.1086/679735* 171:632–645.
43. Gillooly JF, Charnov EL, West GB, Savage VM, Brown JH (2002) Effects of size and temperature on developmental time. *Nature* 417:70–73.
44. Hou C, et al. (2008) Energy Uptake and Allocation During Ontogeny. *Science* 322:736–739.
45. Bettencourt LMA, Lobo J, Helbing D, Kuhnert C, West GB (2007) Growth, innovation, scaling, and the pace of life in cities. *Proc. Natl. Acad. Sci. USA* 104:7301–7306.
46. Folland JP, Mc Cauley TM, Williams AG (2008) Allometric scaling of strength measurements to body size. *Eur J Appl Physiol* 102:739–745.
47. Calder III WA (1983) An allometric approach to population cycles of mammals. *J. Theor. Biol.* 100:275–282.
48. Peterson RO, PAGE RE, DODGE KM (1984) Wolves, Moose, and the Allometry of Population Cycles. *Science* 224:1350–1352.
49. Krukonis G, Schaffer WM (1991) Population cycles in mammals and birds: Does periodicity scale with body size? *J. Theor. Biol.* 148:469–493.
50. Hendriks AJ, Mulder C (2012) Delayed logistic and Rosenzweig{MacArthur models with allometric parameter setting estimate population cycles at lower trophic levels well. *Ecological Complexity* 9:43–54.
51. Kendall BE, et al. (1999) Why do populations cycle? A synthesis of statistical and mechanistic modeling approaches. *Ecology* 80:1789–1805.
52. Högstedt G, Seldal T, Breistol A (2005) Period length in cyclic animal populations. *Ecology* 86:373–378.
53. Kendall, Prendergast, Bjornstad (1998) The macroecology of population dynamics: taxonomic and biogeographic patterns in population cycles. *Ecol. Lett.* 1:160–164.
54. Brown J, Marquet P, Taper M (1993) Evolution of body size: consequences of an energetic definition of fitness. *Am. Nat.* 142:573–584.
55. West GB, Brown JH, Enquist BJ (1997) A General Model for the Origin of Allometric Scaling Laws in Biology. *Science* 276:122–126.
56. West GB, Woodruff WH, Brown JH (2002) Allometric scaling of metabolic rate from molecules and mitochondria to cells and mammals. *Proc. Natl. Acad. Sci. USA* 99:2473–2478.
57. Millar J, Hickling G (1990) Fasting Endurance and the Evolution of Mammalian Body Size. *Funct. Ecol.* 4:5–12.
58. Alroy J (1998) Cope's rule and the dynamics of body mass evolution in North American fossil mammals. *Science* 280:731.
59. Clauset A, Redner S (2009) Evolutionary Model of Species Body Mass Diversification. *Phys. Rev. Lett.* 102:038103.
60. Smith F, Boyer A, Brown J, Costa D (2010) The Evolution of Maximum Body Size of Terrestrial Mammals. *Science*.
61. Saarinen JJ, et al. (2014) Patterns of maximum body size evolution in Cenozoic land mammals: eco-evolutionary processes and abiotic forcing. *Proc Biol Sci* 281:20132049–20132049.
62. Allen AP, Brown JH, Gillooly JF (2002) Global Biodiversity, Biochemical Kinetics, and the Energetic-Equivalence Rule. *Science* 297:1545–1548.
63. Enquist BJ, Brown JH, West GB (1998) Allometric scaling of plant energetics and population density : Abstract : Nature. *Nature* 395:163–165.
64. Tilman D (1981) Tests of Resource Competition Theory Using Four Species of Lake Michigan Algae. *Ecology* 62:802–815.
65. Dutkiewicz S, Follows MJ, Bragg JG (2009) Modeling the coupling of ocean ecology and biogeochemistry. *Global Biogeochem. Cycles* 23:n/a–n/a.
66. Barton AD, Dutkiewicz S, Flierl G, Bragg J, Follows MJ (2010) Patterns of Diversity in Marine Phytoplankton. *Science* 327:1509–1511.

ACKNOWLEDGMENTS. We thank Luis Bettencourt, Jean Philippe Gibert, Eric Libby, and Seth Newsome for helpful discussions and comments on the manuscript. J.D.Y. was supported by startup funds at the University of California, Merced, and an Omidyar Postdoctoral Fellowship at the Santa Fe Institute. C.P.K. was supported by an Omidyar Postdoctoral Fellowship at the Santa Fe Institute. S.R. was supported by grants DMR-1608211 and 1623243 from the National Science Foundation, and by the John Templeton Foundation, all at the Santa Fe Institute.

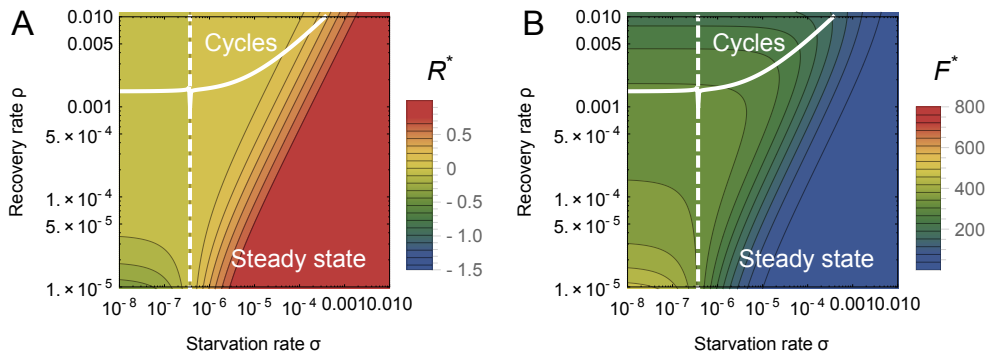

Fig. 1: The transcritical (dashed) and Hopf bifurcation (solid) as a function of the starvation rate σ and recovery rate ρ for a 100g consumer. These bifurcation conditions separate parameter space into infeasible, cyclic, and steady state dynamic regimes. The color gradient shows the steady state densities for (A) the resource R^* and the (B) energetically replete consumers F^*, (warmer colors denote higher densities). Steady state densities for the energetically deficient consumers H^* (not shown) scale with those for F^*.

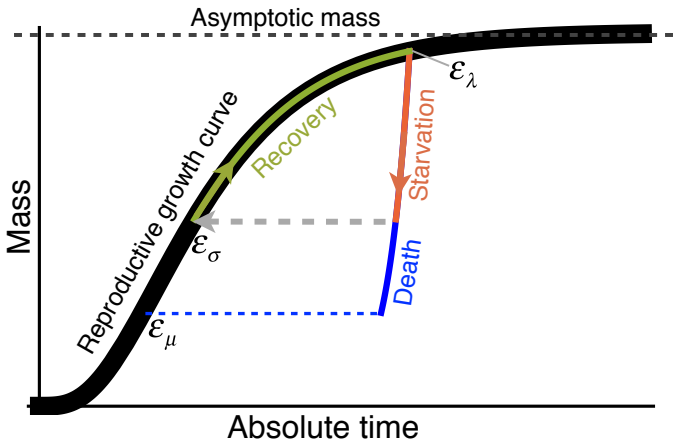

Fig. 2: The growth trajectory over absolute time of an individual organism as a function of body mass. Initial growth follows the black trajectory to an energetically replete reproductive adult mass $m = \epsilon_\lambda M$ which we assume is 95% asymptotic mass M. Starvation follows the red trajectory to $m = \epsilon_\sigma \epsilon_\lambda M$, and recovery follows the green growth trajectory to the replete adult mass. Alternatively, death from starvation follows the blue trajectory to $m = \epsilon_\mu \epsilon_\lambda M$.

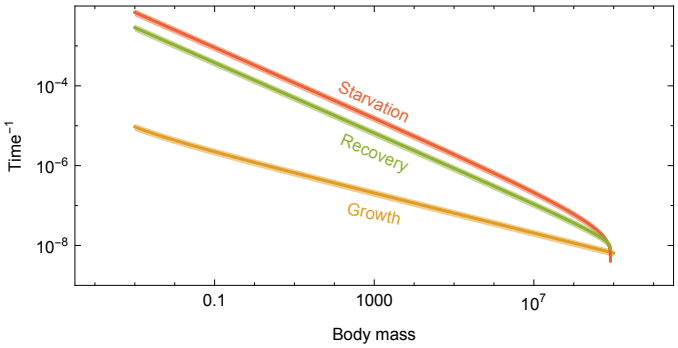

Fig. 3: Allometrically constrained starvation rate σ (red) and recovery rate ρ (green) relative to the reproductive rate λ (orange) as a function of body mass. The rate of starvation is greater than the rate of reproduction for all realized terrestrial endotherm body sizes. Mean values $\pm 20\%$ variation are shown by the shaded region for each rate.

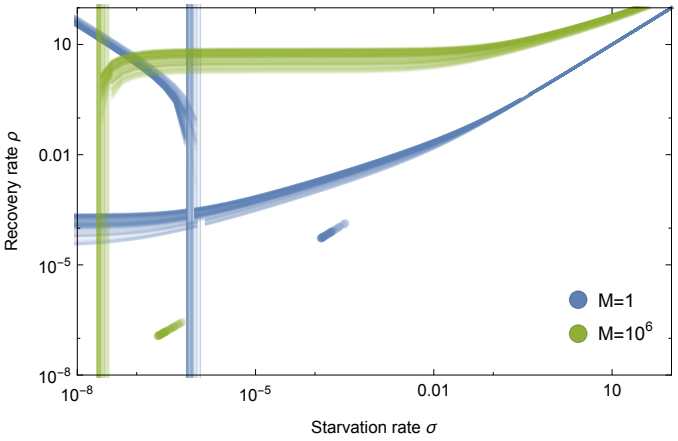

Fig. 4: Transcritical (vertical lines) and Hopf bifurcations (curves) for allometrically determined starvation σ and recovery ρ rates as a function of different mammalian body sizes: $M = A \times 10^{1}$g (blue) and $M = A \times 10^{6}$g (green), where A is a random uniform variable in $[1, 9]$. Points denote realized values of σ and ρ given the drawn values for M.

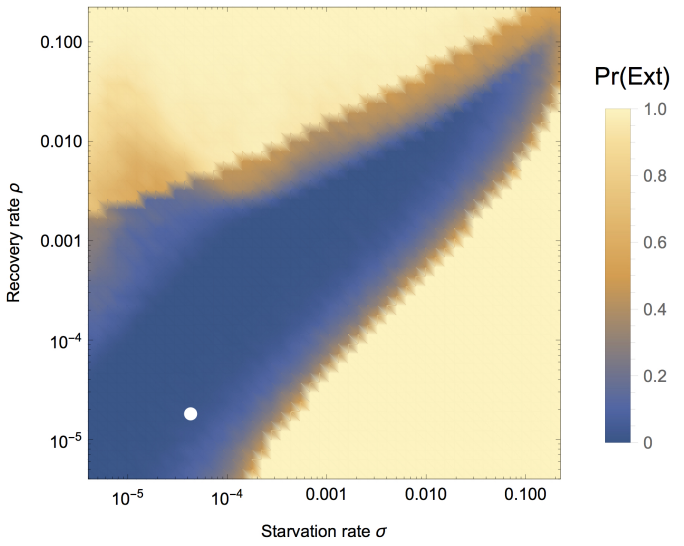

Fig. 5: Probability of extinction for a 100g consumer as a function of the starvation rate σ and recovery rate ρ, where the initial density is given as $A(F^*, H^*, R^*)$, with A being a random uniform variable in $[0, 2]$. Extinction is defined as the population trajectory falling below $0.1\times$ the allometrically constrained steady state. The white point denotes the allometrically constrained starvation and recovery rate.

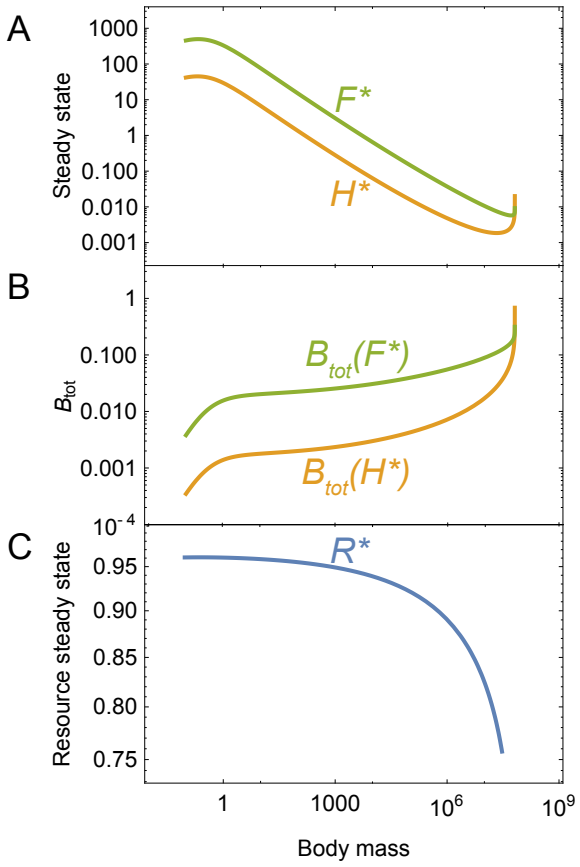

Fig. 6: (A) Consumer steady states F^* (green) and H^* (orange) as a function of body mass. (B) Total energetic use $B_{\rm tot}$ of consumer populations at the steady state as a function of body mass. (C) Resource steady state R^* as a function of consumer body mass.

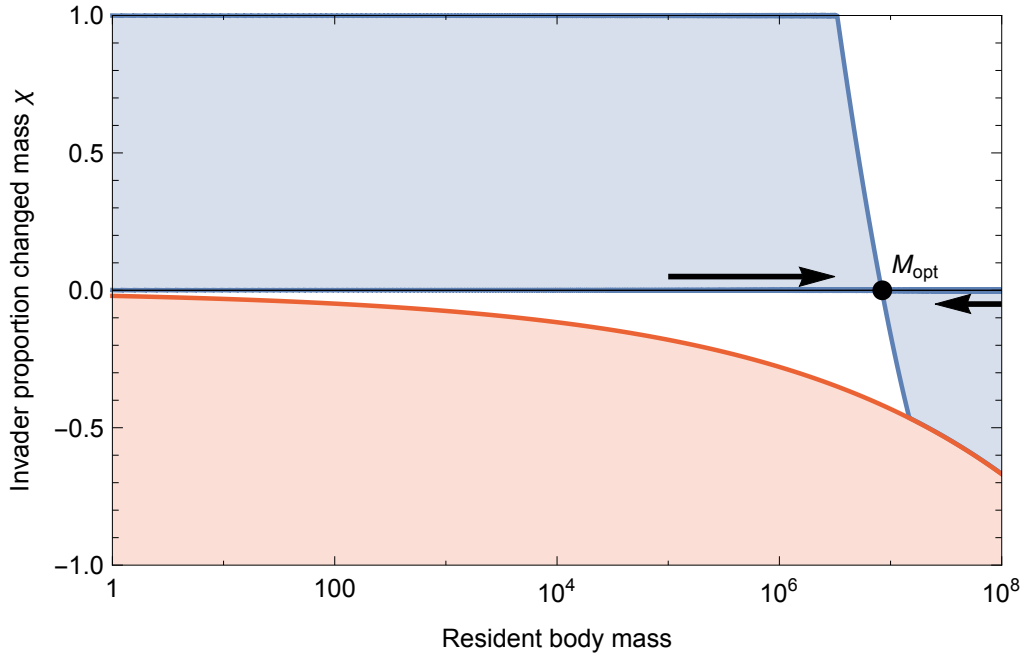

Fig. 7: Invasion feasibility for organisms with a proportional change in mass χ against a population with a resident body mass M. The blue region denotes proportions of modified mass χ resulting in successful invasion. The red region denotes values of χ that result in a mass that is below the starvation threshold and is thus infeasible. Arrows point to the predicted optimal mass $M_{\text{opt}} = 8.43 \times 10^6$, which serves as the uninvadable, evolutionary stable state.